RSC Advances

PAPER

View Article Online
View Journal | View Issue

Cite this: *RSC Adv.*, 2020, **10**, 32897

Formononetin in Radix Hedysari extract-mediated green synthesis of gold nanoparticles for colorimetric detection of ferrous ions in tap water†

Xinyue Chen,[a] Jiahui Ji,[a] Gengen Shi,[a] Zhiyuan Xue,[a] Xianglin Zhou,[a] Lianggong Zhao*[b] and Shilan Feng *[a]

Received 29th June 2020
Accepted 20th August 2020

DOI: 10.1039/d0ra05660j

rsc.li/rsc-advances

This study linked natural plant materials and nanomaterials; reporting an environmentally friendly, non-toxic and efficient method for the green synthesis of gold nanoparticles (AuNPs) using an ethyl acetate extract of Radix Hedysari (EAR). The components of the extract were identified using HPLC and it was found that formononetin accounted for more than 90% of the total contents. We predicted that formononetin in EAR plays a crucial role in green synthesis. Thus, formononetin was used as a standard reductant to synthesize AuNPs, and the result confirmed our prediction. The synthetic mechanism was also discussed in detail in the article. Moreover, EAR–AuNPs realized the sensitive and selective colorimetric detection of ferrous ions (Fe^{2+}) among other metal ions, and were applied to spiked tap water with a low detection limit of 1.5 μM in a wide range from 10 μM to 500 μM. EAR–AuNPs were green synthesized using Radix Hedysari extract for the first time and were successfully applied in real sample detection.

1 Introduction

Gold nanoparticles (AuNPs) have attracted tremendous attention due to their exciting optical properties, unique physicochemical properties and potential applications, ranging from optoelectronics to theragnostics.[1,2] Various methods have been developed to synthesize and stabilize AuNPs, such as chemical, photochemical, sonochemical and electrochemical methods,[3–5] in which chemical methods have been extensively used due to their simplicity.[6] However, chemical methods suffer from drawbacks of toxic reagents and bad biocompatibility,[7] and can be considered to be harmful to human health and environmentally unfriendly.[8] Thus, developing green synthetic methods for AuNPs increases the applicability of nanoscience.[9] As an excellent candidate for the green synthesis of AuNPs, plant extracts and their individual ingredients have attracted much attention from researchers due to the advantages of no toxicity, efficiency, low cost and renewability.[10] However, in most cases, the mechanism and the ingredients which are responsible for the green AuNPs synthesis remain to be elucidated.[11] It has been supposed that common components in plants such as amino acids, phenols, organic acids, flavonoids, alkaloids, polyphenols, terpenoids, heterocyclic compounds, and polysaccharides, act as reducing agents, as well as stabilizing agents for AuNPs.[12,13] Meanwhile, the surface of AuNPs may be functionalized by various components in natural plants.

Radix Hedysari, the main root of *Hedysarum polybotrys* Hand.-Mazz., is a well-known Chinese herbal plant belonging to the Fabaceae family.[14] Radix Hedysari has been widely used in daily life not only as a dietary supplement and seasoning,[15,16] but also as a traditional Chinese medicine for the treatment of diarrhoea, diabetes mellitus, chronic nephritic proteinuria, and inflammation.[17–19] This is owing to the various ingredients contained in Radix Hedysari such as polysaccharides, flavonoids, ginsenoside, trace elements and amino acids,[20] which are beneficial to human health. In particular, flavonoids have proven antioxidant activity in *in vivo* and *in vitro* experiments by many researchers. They exhibit strong antioxidant capacities through scavenging oxygen free radicals, promoting antioxidizers, or inhibiting oxidative enzymes.[21] Depending on their structural characteristics, flavonoids are classified into six categories which share the same basic structure of 2-phenylchromogen.[22] Flavonoids have different conjugations and varying numbers of hydroxyl groups, which enable them to act as reducing agents, as hydrogen- or electron-donating species.[23] Take formononetin for example, the phenolic hydroxyl group at the C_7 position (C_7–OH) is the active site of the formononetin molecule, which can increase the antioxidant activity and reducing capacity of the molecule itself.[24] Therefore, we synthesize AuNPs using the flavonoid compounds in Radix Hedysari extracts and explore its excellent optical properties.

[a]*Institute of Pharmaceutical Analysis, School of Pharmacy, Lanzhou University, Lanzhou, 730000, P. R. China. E-mail: fengshl@lzu.edu.cn; chenxinyue888@126.com; 13636442199@163.com; shigg18@lzu.edu.cn; 13679449239@163.com; 1195533044@qq.com; Tel: +86 931 8915686*

[b]*The Second Hospital of Lanzhou University, Lanzhou, 730030, P. R. China. E-mail: lzxtj2008@hotmail.com; Tel: +86 931 8942460*

† Electronic supplementary information (ESI) available. See DOI: 10.1039/d0ra05660j

In this article, we designed and prepared green synthetic AuNPs using an ethyl acetate extract of Radix Hedysari (EAR). The composition of the extract was identified using high performance liquid chromatography (HPLC), and it was surprisingly found that more than 90% of the composition was formononetin. To clarify the synthetic mechanism, the formononetin standard was also attempted and AuNPs were successfully obtained. The result indicates that the formononetin in EAR plays a crucial role in the green synthesis of AuNPs. The possible mechanism was also discussed. Meanwhile, as a sensitive optical sensor, the synthesized EAR–AuNPs were used to detect ferrous ions (Fe^{2+}) which is a heavy metal environmental pollutant and is harmful to human health. Finally, the EAR–AuNPs realized rapid, sensitive and selective colorimetric detection of Fe^{2+} among various metal ions. The detection mechanism was explored and the synthesized EAR–AuNPs were further applied into the spiked tap water with the detection limit of 1.5 μM. In conclusion, our study developed the potential of traditional herbal plants, creatively linking them to nanomaterials.

2 Experimental section

2.1 Chemicals and reagents

The roots of Radix Hedysari were purchased from Longnan, Gansu Province and identified by Professor Zhigang Ma at Lanzhou University. Chloroauric acid ($HAuCl_4 \cdot 3H_2O$) was purchased from Sigma-Aldrich (USA) and applied directly. Formononetin was purchased from Aladdin Bio-Chem Technology Co., Ltd (Shanghai, China). Metal-salts of $Al(NO_3)_3$, $AgNO_3$, Cr_2O_3, $FeCl_3$, KCl, $FeSO_4 \cdot 7H_2O$, $CuCl_2$, NaCl, $NiCl_2$, $Zn(NO_3)_2$, and $Pb(NO_3)_2$ were purchased from Baishi Chemical Co., Ltd (Tianjin, China). All the experimental solutions were prepared using distilled water and all chemicals involved in this study were of analytical reagent grade.

2.2 Preparation of the ethyl acetate extract of Radix Hedysari

The ethyl acetate extract of Radix Hedysari (EAR) was prepared according to our previous work.[15,16] In brief, dried Radix Hedysari powder was extracted with 6-fold ethyl acetate 3 times, 2 h each time. All of the extracting solutions were merged and vacuum recycled to obtain the dried ethyl acetate extract, which was stored under appropriate conditions before use.

2.3 Preparation of AuNPs using different reductants

2.3.1 Preparation of different sized AuNPs using the ethyl acetate extract. Different sized AuNPs were green synthesized using EAR (EAR–AuNPs), in which EAR also acted as the stabilizer and modifier. 0.15 g of EAR was dissolved into 1 mL of ethanol to ensure the solubility and dispersion of the solution. 0.1 mL, 0.25 mL, 0.5 mL, 1 mL, or 1.5 mL of the solution were added into a boiling $HAuCl_4$ solution (20 μL of 10% $HAuCl_4$ dissolved into 50 mL distilled water) under vigorous stirring. The mixed solutions were kept boiling for 15 min and then cooled to room temperature to obtain the different sized EAR–AuNPs solutions.

2.3.2 Preparation of AuNPs using formononetin standard. AuNPs were synthesized by formononetin standard. 20 mg of formononetin standard was dissolved into 4 mL of ethanol to obtain the solution with good solubility. Then the solution was added into the boiling $HAuCl_4$ solution as mentioned above. The color of the resulting solution was purple.

2.4 Characterization of EAR–AuNPs

The composition of EAR was identified using a Waters 2695 high performance liquid system (HPLC), including 717 autosampler manager and 2996 UV detector, connected to Millennium 32 software (Waters, USA). HPLC conditions were as follows: a Spursil C18 column (250 × 4.6 mm, 5 μm) was used. The mobile phase was formed by solvent A (acetonitrile) and solvent B (water solution) with a linear gradient as follows: 0–30 min: 30% A, 30–65 min: 60% A. The flow rate was 1.0 mL min^{-1}, column temperature was 30 °C and injection volume was 20 μL. The spectrum was monitored at 280 nm.

Fourier transform infrared (FT-IR) spectra were conducted on a Nicolet NEXUS-870 FT-IR spectrometer (Thermo Nicolet, USA). An ultraviolet spectrometer (UV-vis, Perkin Elmer, USA) equipped with a 1 cm-path-length quartz cell was operated to obtain the UV-vis spectrum. The size of AuNPs was confirmed on the laser dynamic scattering instrument Zetasizer Nano 3600 (Malvern, UK). Transmission electron microscopy (TEM) images were measured on an FEI Tecnai G2TF20 instrument (FEI-TECNAI, USA) operating at an acceleration voltage of 200 kV. The laser dynamic scattering instrument, Zetasizer Nano 3600 (DLS, Malvern, UK), was used to record the size of nanoparticles in the solution.

2.5 The optimization of external conditions

The external conditions such as pH and temperature were optimized to improve the analytical merit of synthesized EAR–AuNPs. To select the optimal reaction temperature, the synthesized AuNPs solution was placed at temperatures varying from 20 °C to 80 °C. To choose the optimal pH value, the EAR–AuNPs solution was adjusted over pH 1–14.

2.6 Analytical merit of EAR–AuNPs for sensing Fe^{2+}

Under optimal external conditions (pH value of 6, temperature of 20 °C), EAR–AuNPs were prepared for the sensitive detection of Fe^{2+}. 40 μL of different concentrations of Fe^{2+} were added into 360 μL of freshly prepared EAR–AuNPs solution (characteristic absorption at 540 nm). The final concentrations of the solutions were 10 μM, 25 μM, 50 μM, 100 μM, 500 μM and 1 mM. After vortex blending for 10 s, the mixture was kept for 10 min to observe the color change.

To explore the selectivity of EAR–AuNPs, the sensor was prepared for the detection of Fe^{2+} among 10 other metal ions. 40 μL of different metal ion solutions (Pb^{2+}, K^+, Fe^{2+}, Cu^{2+}, Fe^{3+}, Zn^{2+}, Ni^{2+}, Na^+, Cr^{3+}, Ag^+) were added into 360 μL of EAR–AuNPs solution with the same concentration of 100 μM. The experiment was conducted in the same way as above, to observe the color change and record the Uv-vis spectrum.

To explore the anti-interference performance of EAR–AuNPs, the sensor was prepared to detect Fe^{2+} in the presence of other metal ions. 20 μL of Fe^{2+} solution was added into 360 μL of EAR–AuNPs solution mixed with 20 μL of different metal ion solutions (Pb^{2+}, K^{+}, Cu^{2+}, Fe^{3+}, Zn^{2+}, Ni^{2+}, Na^{+}, Cr^{3+}, Ag^{+}). The concentration of each metal ion is 100 μM. The experiment was conducted in the same way as above.

2.7 Real sample detection

To further investigate the application of EAR–AuNPs, the same experiment was used again to detect Fe^{2+} in tap water. The tap water sample was collected at the School of Pharmacy, Lanzhou University. A series of Fe^{2+} standard solutions were directly spiked into the tap water samples. 40 μL of spiked tap water was added into 360 μL of EAR–AuNPs solution, the mixture was continuously vortex-blended for 20 s and then incubated for 10 min to observe the color change. The final concentrations were 10 μM, 25 μM, 100 μM, 500 μM and 1 mM.

3 Results and discussion

3.1 Comparison of synthesized EAR–AuNPs

AuNPs with various sizes were green synthesized by adding different contents of EAR solution. The color of EAR–AuNPs solutions are shown in Fig. 1A, and the corresponding characteristic absorption peaks were 570 nm, 544 nm, 540 nm, 538 nm, 548 nm, respectively. The UV-vis of the EAR solution is also shown in Fig. S1† to remove the interference of the solvent. EAR–AuNPs solutions with characteristic absorption peaks at 544 nm, 540 nm, and 538 nm were almost uniform in their purple color. While EAR–AuNPs with characteristic absorption peaks at 548 nm or 570 nm were gray in solution, indicating large-sized AuNPs were obtained, which are probably unsuitable for colorimetric detection. This is due to the narrow visual range. The naked eye can easily recognize the color change from red/purple to gray or clear, while it is less likely to recognize the change from gray to clear or a darker grey. Besides, the stability of the large-sized EAR–AuNPs was poor, especially at high temperature or a strong acid/alkali environment. The TEM images of the different-sized EAR–AuNPs are shown in Fig. S2 and S3.† It was found that most nanoparticles at a maximum absorption wavelength of 540 nm were relatively regular. Individual particles, were irregular, this was because Radix Hedysari has a variety of ingredients rather than a single one, which react differently with chemical reagents. However, at other maximum absorption wavelengths, the morphology of most nanoparticles was irregular. Therefore, the purple EAR–AuNPs solution with characteristic absorption peak at 540 nm was selected for subsequent experiments to explore its detection performance. And the above experimental results proved the reducing ability of EAR.

3.2 Mechanism for green synthesis

In order to clarify the green synthesis mechanism for EAR–AuNPs, HPLC was first applied to identify the components of EAR. By comparing the retention time and characteristic UV-vis spectrum between the EAR sample (Fig. 2A) and formononetin (Fig. 2B) standard solution, the formononetin compound in EAR was unambiguously identified. It is worth noting that the content of formononetin accounted for more than 90% of the total content of EAR through the quantitative statistics. Therefore, we supposed that formononetin in EAR has reducing ability and played a major role in the green synthesis. To prove this hypothesis, the standard formononetin was also added into a boiling solution of $HAuCl_4$ under the same conditions to observe the change. The reaction product is shown in the Fig. 1B. The color of solution was purple with the characteristic absorption peak was at 560 nm. The TEM image is shown in Fig. S4.† The results indicate that the standard formononetin has reducing ability and could be used to synthesize AuNPs, further confirming that formononetin in EAR plays a crucial role in the green synthesis of EAR–AuNPs. Formononetin is one of the major flavonoids with strong antioxidant capacities which has been proved through a series of reactions that could scavenge oxygen free radicals. Formononetin has the common structure of 2-phenylchromogen which is shared by all flavonoids. The varying number of hydroxyl groups in flavonoid structures enables them to act as reducing agents, as hydrogen- or electron-donating species oxidative enzymes.[23] In the structure of formononetin, the phenolic hydroxyl group at the C_7 position (C_7–OH) is the active site, significantly improving the antioxidant activity and reducing capacity of the molecule itself. Thus Au(III) could be reduced to Au(0) by formononetin owing to its reductive group. Through HPLC identification, it could be

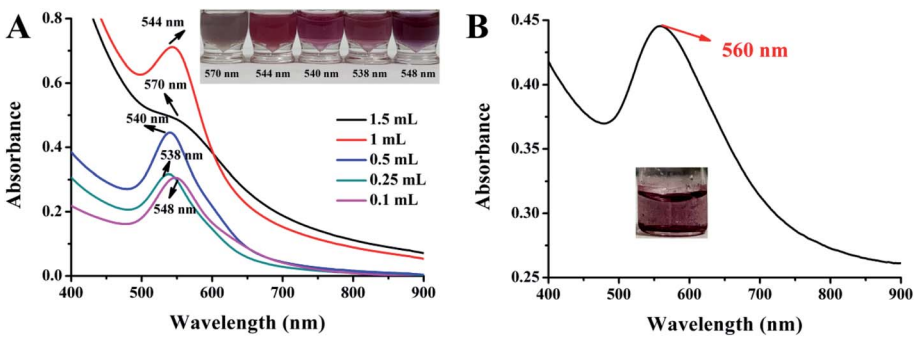

Fig. 1 Photographs and normalized UV-vis absorption spectra of (A) various EAR–AuNPs synthesized by adding different contents of EAR, and (B) AuNPs synthesized by formononetin standard with characteristic absorption peaks.

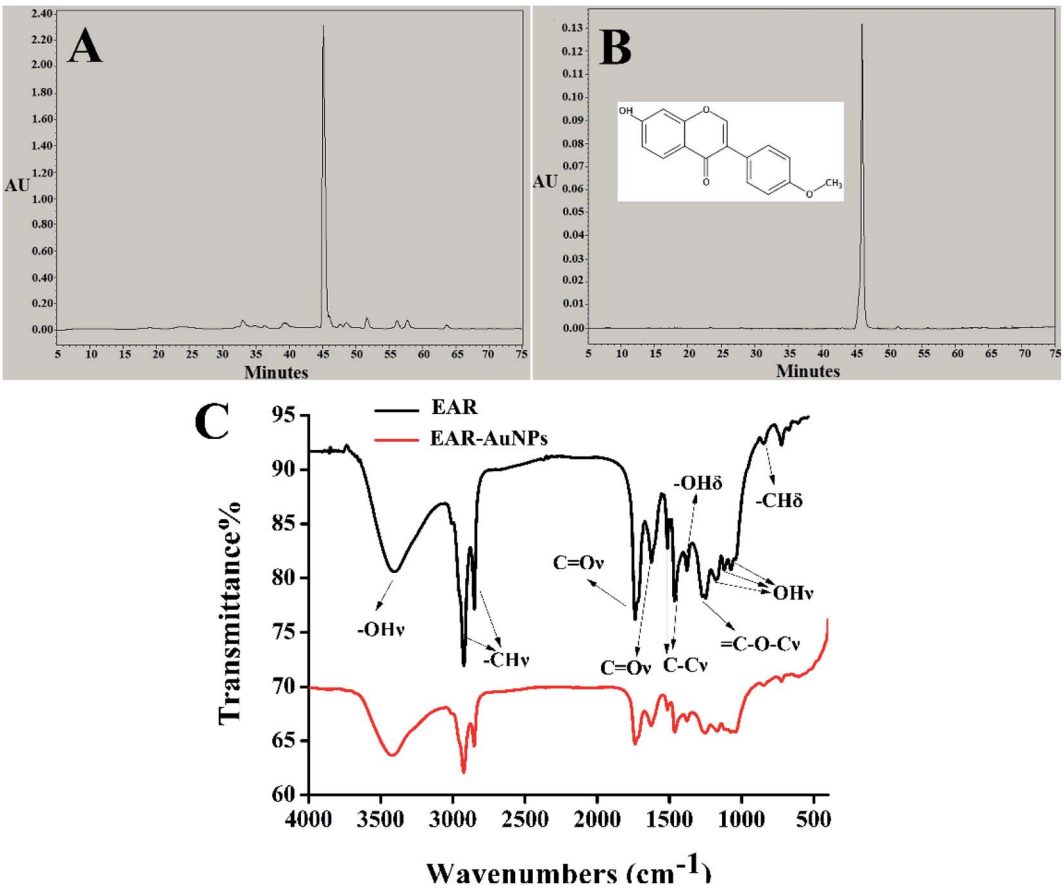

Fig. 2 HPLC spectrum of (A) EAR and (B) formononetin standard. (C) The FT-IR spectra of EAR and EAR–AuNPs.

clearly observed that formononetin in the extract plays a primary function in the green synthesis of EAR–AuNPs.

3.3 Characterization of EAR–AuNPs

In the FT-IR spectrum (Fig. 2C), the absorption peaks of EAR were identified as the O–H stretching vibration at 3405 cm^{-1}, C–H stretching vibration at 2924 and 2852 cm^{-1}, C=O stretching vibration at 1737 and 1624 cm^{-1}, C–C stretching vibration at 1514 and 1464 cm^{-1}, O–H bending vibration at 1378 cm^{-1}, =C–O–C stretching vibration at 1270 and 1249 cm^{-1}, O–H stretching vibration at 1178, 1120 and 1073 cm^{-1}, C–H bending vibration at 846 cm^{-1}, which are almost consistent with the characteristic groups of the formononetin standard. Thus, it is worth noting that formononetin accounted for the majority of the total content in EAR. The result further confirmed the main structure of EAR and the successful synthesis of EAR–AuNPs.

3.4 Analytical merit of EAR–AuNPs

3.4.1 Optimization of external conditions. External conditions have considerable influence on the detection performance of AuNPs, thus it is crucial to optimize the external conditions

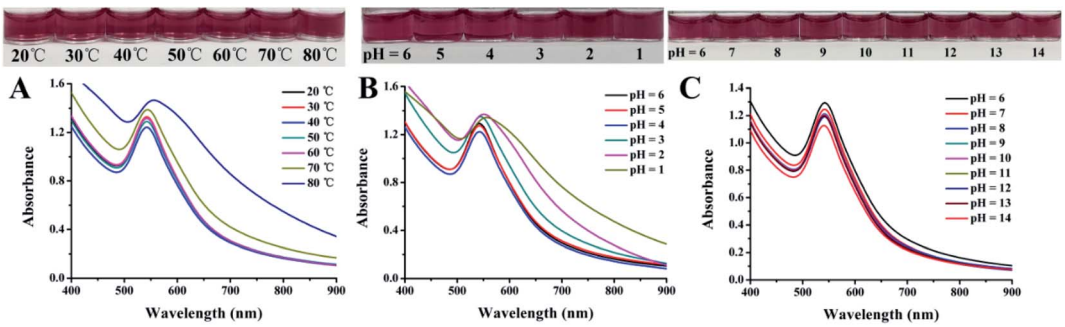

Fig. 3 Photographs and normalized UV-vis absorption spectra for EAR–AuNPs under (A), different temperatures and (B), (C) different pH values.

such as temperature and pH value. As shown in Fig. 3A, the synthesized EAR-AuNPs were subjected to a series of temperatures ranging from 20–80 °C. The color change was observed and the UV-vis spectrum was recorded. It was found that when the temperature was above 60 °C, the EAR–AuNPs became unstable, leading to the color change and red-shift of the characteristic absorption peak. This change became more obvious when the temperature reached 80 °C. Therefore, EAR–AuNPs could remain stable in the range 20 °C to 60 °C, and the temperature should be kept below 60 °C during the experiment to guarantee the reaction.

To investigate the influence of temperature, the EAR solutions were kept at 60 °C, 70 °C, 80 °C, respectively and then freeze-dried into powder to obtain FT-IR spectrograms. The FT-IR spectrograms of different EAR solutions are shown in Fig. S5.† It was found that characteristic functional groups in EAR did not change at different temperatures, indicating that changes in temperature had little effect on EAR itself. As for

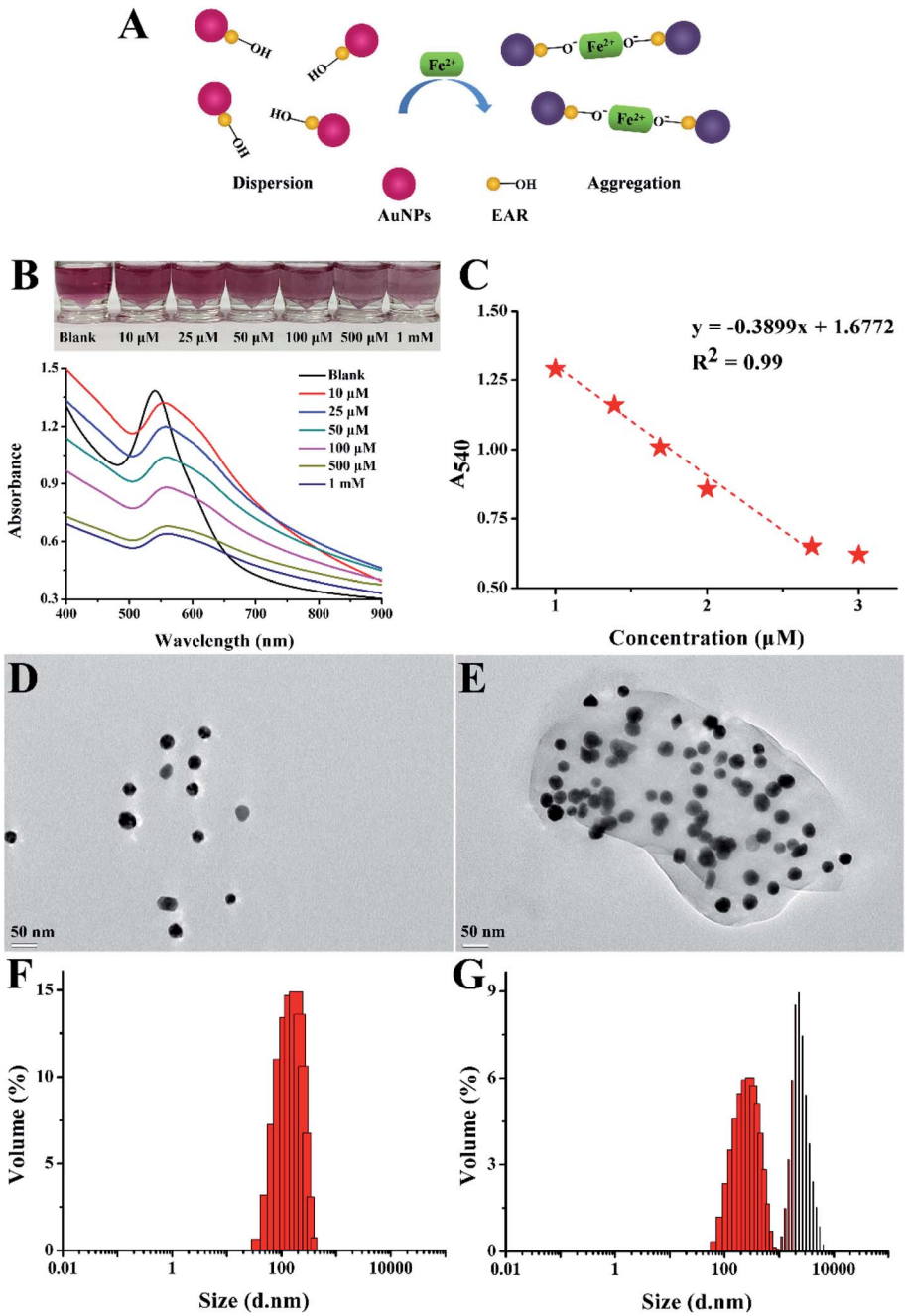

Fig. 4 (A) The possible mechanism of the colorimetric sensing of Fe^{2+} using EAR–AuNPs. (B) Photographs and normalized UV-vis absorption spectra of EAR–AuNPs added by a series concentration of Fe^{2+}. (C) The correlation between Fe^{2+} concentration and absorbance. A dynamic response toward A_{540} over the logarithm of concentration corresponding to (B). TEM results of (D) dispersed EAR–AuNPs and (E) aggregated EAR–AuNPs. Size distribution of (F) dispersed EAR–AuNPs solution and (G) aggregated EAR–AuNPs solution detected by DLS.

EAR–AuNPs, they have small particle size and large specific surface area, causing a large surface free energy in the nano system. Therefore, gold nanoparticles are in a high energy state which is thermodynamically unstable. They can spontaneously agglomerate, oxidize or adsorb on the surface to reduce the number of unstable atoms on the surface, so as to reduce the energy of the system. We hypothesized that the high temperature condition could increase the thermodynamic instability of the nanoparticles and stimulate the surface free energy of the particles, thus leading to aggregation to reduce the system energy. Therefore, gold nanoparticles showed instability with the increase in temperature.

The pH values of EAR–AuNPs were adjusted from 1–14 to observe the color change and UV-vis spectrum. As shown in Fig. 3B, when the pH value varied from 6 to 1, the color of the solution gradually darkened as the pH value gradually decreased, especially when it was below 4. The UV-vis spectrum was also gradually red-shifted. When the pH value changed within the range 6–14, the color of the EAR–AuNPs solution basically remained unchanged, which is consistent with the UV-vis spectrum (Fig. 3C). The activity of EAR–AuNPs decreased slightly when the pH value was above 13. The result indicates that EAR–AuNPs were prone to instability in acidic solution, and the pH value of solution should be higher than 4.

Under acidic conditions, the concentration of hydrogen ions in the solution is high, and is prone to electrostatic attraction with the negative charge on the surface of EAR–AuNPs, leading to aggregation of the nanoparticles. Therefore, as at lower pH values, the concentration of hydrogen ions in the solution is higher, and EAR–AuNPs would be more unstable.

3.4.2 Sensitivity of colorimetric detection for Fe^{2+}. The analytical merit of EAR–AuNPs for Fe^{2+} detection was investigated under optimal conditions. The possible mechanism for colorimetric sensing of Fe^{2+} is exhibited in Fig. 4A. The complexing action between the lone pair electrons on the hydroxide radical and Fe^{2+} occurred, which shortens the distance between particles, leading to the aggregation of AuNPs and the color change of solution. The result in Fig. 4B further confirmed this hypothesis. A series of concentrations of Fe^{2+} was added into the EAR–AuNPs solution and the color of the solution was

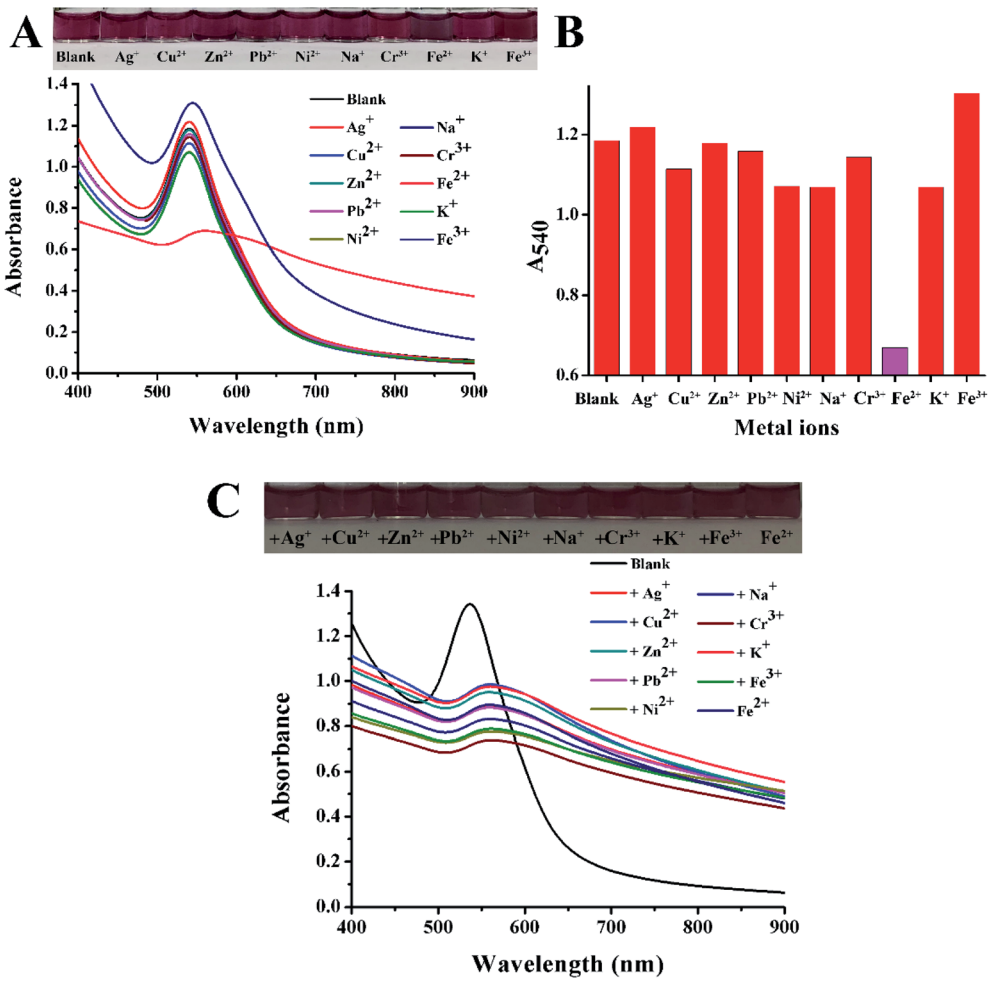

Fig. 5 (A) Photographs and UV-vis absorption spectra of EAR–AuNPs with the addition of different kinds of metal ions. The concentration of each was 100 μM. (B) Histogram of absorbance at 540 nm after adding Fe^{2+} corresponding to the spectrum in (A). (C) Photographs and UV-vis absorption spectra of EAR–AuNPs with the addition of 100 μM Fe^{2+} and other kinds of metal ions. The concentration of each was 100 μM.

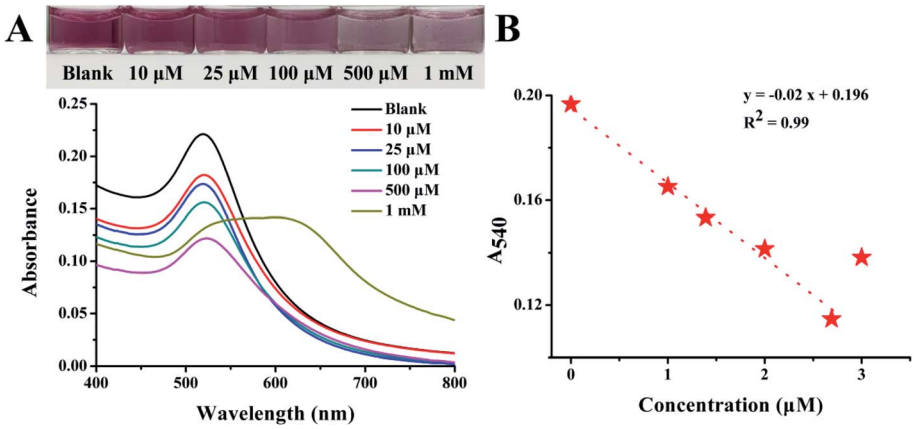

Fig. 6 (A) Photographs and UV-vis absorption spectra of EAR–AuNPs after the addition of tap water spiked with various concentrations of Fe^{2+}. (B) The correlation between spiked tap water and absorbance. A dynamic response toward A_{540} over the logarithm of concentration corresponding to (A).

observed. With the increasing target concentration, the color of the solution gradually changed from purple to gray, and the characteristic absorption peak shifted from 540 nm to 560 nm, indicating the formation of aggregates. Accordingly, the colorimetric response at an absorption of 540 nm (A_{540}) was introduced to illustrate the accurate quantitative determination of Fe^{2+}. The result is shown in Fig. 4C, a linear regression between the A_{540} and a series concentration of Fe^{2+} was established where $y = -0.3899x + 1.6772$ in the range of 10 μM–500 μM with a correlation coefficient (R^2) of 0.99. TEM (Fig. 4D and E) and DLS results (Fig. 4F and G) also confirmed the changes of morphology and size of EAR–AuNPs in the absence or presence of Fe^{2+}. Without the addition of the target, the EAR–AuNPs were homogeneous and monodisperse with good stability. While the addition of Fe^{2+} could trigger the aggregation of EAR–AuNPs, leading to the change of particle morphology and the increase of particle size. In the DLS result, it was worth noting that the particle size of EAR–AuNPs is much larger than that in TEM. This was mainly because the TEM measured the actual size at the dried state of sample, while DLS measured a hydrodynamic diameter (hydrated state), and therefore the AuNPs showed a larger hydrodynamic volume due to the solvent effect in the hydrated state.[25]

3.4.3 Selectivity and anti-interference performance of EAR–AuNPs. To ensure the application of EAR–AuNPs in real samples, the selectivity and anti-interference performance of EAR–AuNPs for Fe^{2+} were also investigated. The same concentration of 100 μM of various metal ions were added into the above EAR–AuNPs solution. As shown in Fig. 5A, When Fe^{2+} was added, the color of the solution changed from purple to grey with the characteristic absorption peak shift from 540 nm to 560 nm. While the rest of the solutions added containing other metal ions exhibited no obvious color change with the characteristic absorption peak remaining almost the same. However, in the presence of other metal ions, the same concentration of Fe^{2+} was also detected, accompanied with the obvious color change and red-shift of the characteristic absorption peak (Fig. 5C), which indicated the good anti-interference performance of EAR–AuNPs. The statistical result of the histogram shown in Fig. 5B further exhibits that there was a clear difference between Fe^{2+} and the other metal ions. Fe^{2+} could induce the complexing action, leading to the aggregation of nanoparticles. The result indicated that among the many common metal ions, Fe^{2+} could be sensitively and selectively determined by EAR–AuNPs.

3.4.4 Real sample detection. In order to investigate the practical use of EAR–AuNPs, they were applied to spiked tap water. A series concentration of Fe^{2+} was dissolved in tap water to obtain the spiked samples with final concentrations of 10 μM, 25 μM, 100 μM, 500 μM, 1 mM. Then the spiked tap water samples were added into EAR–AuNPs solutions to observe the color change. As shown in Fig. 6A, with increasing Fe^{2+} concentration, the color of the solution gradually changed from purple to gray and the UV-vis spectrum red-shifted. The calibration curve was obtained by plotting the absorbance value at 540 nm (A_{540}) against concentration. According to the statistical result, the calibration curve is linear over the range from 10 μM to 500 μM with the regression equation $A_{540} = -0.02x + 0.196$, and correlation coefficient R^2 of 0.99 (Fig. 6B). The detection limit (LOD) observed by the naked eye was 10 μM while the calculated value was determined to be 1.5 μM based on the formula: $LOD = 3\sigma/s$, in which σ represents the blank standard deviation and s represents the slope of the linear regression equation.[26]

4 Conclusions

Such EAR–AuNPs has the following benefits and applications: (1) the EAR–AuNPs were green synthesized with the ethyl acetate extract of Radix Hedysari for the first time, which was eco-friendly and had good biocompatibility compared with toxic chemical methods. (2) This work provided a sensitive and selective detector for Fe^{2+} over various other metal ions, which was successfully applied to spiked tap water. (3) The components of EAR were identified by HPLC and formononetin accounted for more than 90%, which provided strong evidence

to illustrate the synthetic and detection mechanism of EAR–AuNPs. (4) We developed the potential of traditional Chinese medicine and expanded its practical application.

Conflicts of interest

The authors declare that they have no competing interests.

Acknowledgements

The authors greatly appreciate financial support from the National Natural Science Foundation of China (No. 81703664) and the China Postdoctoral Science Foundation (No. 415249).

References

1 S. Mondal, U. Rana, R. R. Bhattacharjee and S. Malik, One pot green synthesis of polyaniline coated gold nanorods and its applications, *RSC Adv.*, 2014, **4**, 57282–57289.
2 W. Wang, J. Li, S. Lan, L. Rong, Y. Liu, Y. Sheng, H. Zhang and B. Yang, Seedless synthesis of gold nanorods using resveratrol as a reductant, *Nanotechnology*, 2016, **27**(16), 165601–165611.
3 P. Uznanski and E. Bryszewska, Synthesis of silver nanoparticles from carboxylate precursors under hydrogen pressure, *J. Mater. Sci.*, 2010, **45**(6), 1547–1552.
4 S. Joseph and B. Mathew, Microwave assisted facile green synthesis of silver and gold nanocatalysts using the leaf extract of Aerva lanata, *Spectrochim. Acta Mol. Biomol. Spectrosc.*, 2015, **136**, 1371–1379.
5 N. Abdel-Raouf, N. M. Al-Enazi and I. B. Ibraheem, Green biosynthesis of gold nanoparticles using Galaxaura elongata and characterization of their antibacterial activity, *Arabian J. Chem.*, 2017, **10**, S3029–S3039.
6 S. Link and M. A. El-Sayed, Spectral properties and relaxation dynamics of surface plasmon electronic oscillations in gold and silver nanodots and nanorods, *J. Phys. Chem. B*, 1999, **103**, 8410–8426.
7 M. Dhayalan, M. I. J. Denison, M. Ayyar, N. N. Gandhi, K. Krishnan and B. Abdulhadi, Biogenic synthesis, characterization of gold and silver nanoparticles from Coleus forskohlii and their clinical importance, *J. Photochem. Photobiol. B Biol.*, 2018, **183**, 251–257.
8 A. A. Kajani, A.-K. Bordbar, S. H. Zarkesh Esfahani and A. Razmjou, Gold nanoparticles as potent anticancer agent: green synthesis, characterization, and in vitro study, *RSC Adv.*, 2016, **6**, 63973–63983.
9 M. Hamelian, K. Varmira and H. Veisi, Green synthesis and characterizations of gold nanoparticles using Thyme and survey cytotoxic effect, antibacterial and antioxidant potential, *J. Photochem. Photobiol. B Biol.*, 2018, **184**, 71–79.
10 K. J. Rao and S. Paria, Green synthesis of gold nanoparticles using aqueous Aegle marmelos leaf extract and their application for thiamine detection, *RSC Adv.*, 2014, **4**, 28645–28652.
11 P. Singh, Y.-J. Kim, D. Zhang and D.-C. Yang, Biological synthesis of nanoparticles from plants and microorganisms, *Trends Biotechnol.*, 2016, **34**(7), 588–599.
12 H. Duan, D. Wang and Y. Li, Green chemistry for nanoparticle synthesis, *Chem. Soc. Rev.*, 2015, **44**(16), 5778–5792.
13 F. J. Osonga, I. Yazgan, V. Kariuki, D. Luther, A. Jimenez, P. Le and O. A. Sadik, Greener synthesis and characterization, antimicrobial and cytotoxicity studies of gold nanoparticles of novel shapes and sizes, *RSC Adv.*, 2016, **6**, 2302–2313.
14 L. Zhao, H. Zhao, X. Sheng, T. Chen, Z. Dang, L. An, J. Ma, S. Feng and Y. Xia, Structural characterization and stimulating effect on osteoblast differentiation of a purified heteropolysaccharide isolated from Hedysarum polybotrys, *Carbohydr. Polym.*, 2014, **111**, 714–721.
15 X. Yang, Z. Xue, Y. Fang, X. Liu, Y. Yang, G. Shi, S. Feng and L. Zhao, Structure–immunomodulatory activity relationships of Hedysarum polysaccharides extracted by a method involving a complex enzyme combined with ultrasonication, *Food Funct.*, 2019, **10**(2), 1146–1158.
16 Z. Xue, G. Shi, Y. Fang, X. Liu, X. Zhou, S. Feng and L. Zhao, Protective effect of polysaccharides from Radix Hedysari on gastric ulcers induced by acetic acid in rats, *Food Funct.*, 2019, **10**(7), 3965–3976.
17 Z. Wang, P. Zhang, Y. Kou, X. Yin, N. Han and B. Jiang, Hedysari extract improves regeneration after peripheral nerve injury by enhancing the amplification effect, *PloS One*, 2013, **8**(7), e76633–e76643.
18 Y. Shi, L. Zhao, X. Liu, F. Hu, F. Cui, Y. Bi, Y. Ma and S. Feng, Structural characterization of a sulfated glucan isolated from the aqueous extract of Hedysarum polybotrys Hand.-Mazz, *Carbohydr. Polym.*, 2012, **87**(1), 160–169.
19 Z. Dang, D. Feng, X. Liu, T. Yang, L. Guo, J. Liang, J. Liang, F. Hu, F. Cui and S. Feng, Structure and antioxidant activity study of sulfated acetamido-polysaccharide from Radix Hedysari, *Fitoterapia*, 2013, **89**, 20–32.
20 X.-Y. Chen, S.-H. Gou, Z.-Q. Shi, Z.-Y. Xue and S.-L. Feng, Spectrum-effect relationship between HPLC fingerprints and bioactive components of Radix Hedysari on increasing the peak bone mass of rat, *J. Pharm. Anal.*, 2019, **9**(4), 266–273.
21 P. Wu, G. Ma, N. Li, Q. Deng, Y. Yin and R. Huang, Investigation of in vitro and in vivo antioxidant activities of flavonoids rich extract from the berries of Rhodomyrtus tomentosa (Ait.) Hassk, *Food Chem.*, 2015, **173**, 194–202.
22 J. Peterson and J. Dwyer, Flavonoids: dietary occurrence and biochemical activity, *Nutr. Res.*, 1998, **18**(12), 1995–2018.
23 M. Zietz, A. Weckmüller, S. Schmidt, S. Rohn, M. Schreiner, A. Krumbein and L. W. Kroh, Genotypic and climatic influence on the antioxidant activity of flavonoids in kale (Brassica oleracea var. sabellica), *J. Agric. Food Chem.*, 2010, **58**(4), 2123–2130.
24 X. Zhang, Y. Yang and Q. Lv, Density functional theory calculations on antioxidation activity of the isoflavone compounds from astragalus, *Chem Res Appl*, 2012, **24**, 1662–1669.

25 W. She, K. Luo, C. Zhang, G. Wang, Y. Geng, L. Li, B. He and Z. Gu, The potential of self-assembled, pH-responsive nanoparticles of mPEGylated peptide dendron-doxorubicin conjugates for cancer therapy, *Biomaterials*, 2013, **34**(5), 1613–1623.

26 X.-Y. Chen, W. Ha and Y.-P. Shi, Sensitive colorimetric detection of melamine in processed raw milk using asymmetrically PEGylated gold nanoparticles, *Talanta*, 2019, **194**, 475–484.